

Using a Half-mode SIW Loaded with Slots to Realize a Compact UWB Bandpass Filter

Hussein Al-Jeshami¹, Hussam Al-Saedi¹, Mohammed F. Hasan¹, Halah I. Khani¹,
Muhannad Y. Muhsin¹, and Wael M. Abdel-Wahab²

¹University of Technology – Iraq, Baghdad, Iraq,

²University of Waterloo, Waterloo, Canada

<https://doi.org/10.26636/jtit.2025.2.2085>

Abstract – This paper presents an ultra-wideband bandpass filter (UWB-BPF) based on a half-mode substrate-integrated waveguide (HMSIW) structure with a passband that spans from 4.12 to 11 GHz and has a center frequency of 7.56 GHz with a fractional bandwidth of 91%. Less than 0.3 dB of insertion loss was achieved through the passband, with the return loss being better than 19 dB. Two transmission zeros were generated, contributing to the 5.24 GHz out-of-band rejection. The proposed filter is compact, making it a good choice for space-constrained systems. In addition, a notch response has been utilized to comply with standards issued by applicable regulatory bodies, by blocking some bands located in the passband. Ansys EDT software was used to implement the design and determine the response of the proposed structure, while Keysight ADS was used to validate the results.

Keywords – compact filter, half-mode SIW, notch response, slots loaded, ultra-wideband

1. Introduction

Ultra-wideband technology (UWB) represents a remarkable step in the development of wireless communication systems. Due to its fractional bandwidth (FBW) of more than 20% [1], it has a wide range of applications and is used, inter alia, in medical imaging, ground penetration radars, surveillance, and portable electronic devices. The importance of UWB devices comes from their role in enhancing overall performance and, thus, increasing the reliability of wireless communication. The latter may be achieved mainly by minimizing interference to maintain integrity of signals.

Many papers focusing on UWB technology have been written. As far as filter design is concerned, the following works are worth mentioning as significant. Multiple UWB filters were discussed in [2], while a single notch UWB bandpass filter (UWB-BPF) was created in [3], [4] by using modified substrate-integrated waveguide (SIW) in combination with a dual-split square complementary split ring resonator (CSRR).

A miniaturized frequency-selective surface with intricate square-shaped rings and grids was presented in [5] to realize a dual-band BPF (DB-BPF). Although it has a compact

size, the high complexity of using cascaded layers is a significant drawback due to the manufacturing tolerances that are achievable at present.

A half-mode SIW-based (HMSIW) resonator loaded with square-shaped slot was presented in [6]. It has a simple structure with a fairly small footprint. However, it provides narrow upper band rejection. In article [7], another SIW-based resonator loaded with U-shaped slots was proposed to illustrate the BPF response. The filter has two notches generated by further loading the resonator with lumped elements (capacitors). This filter is considered large and the design is characterized by poor impedance matching within the operating passband.

In [8], researchers presented an UWB-BPF component using a butterfly-shaped unit cell to load the coplanar waveguide technology. Additionally, T-resonators were added to the structure to obtain a notch response within the passband region. An UWB-BPF using open-stub resonators with stepped impedance is discussed in [9].

The resonators take advantage of using multimode quarter-wavelength series transformers. A defected ground structure (DGS) in a bowtie-shaped pattern and a grid of multi slots were engraved on the top layers of an SIW resonator to produce an UWB-BPF response in [10], while a combination of spoof surface plasmon polaritons (SSPP) and HM-SIW were used to form UWB-BPF response for Ka- and X-band applications in papers [11], [12].

A quasi-lumped SIW cavity was proposed in [13], despite its high-profile structure, because many SMD capacitors were integrated on the top layer to reduce the overall size. In [14], the researchers realized a hybrid fractal slot on the top of a HM-SIW resonator with the help of a square-ring CSRR unit cell, such as DGS, to create a BPF structure, while fractal-based miniaturization with meander line slots was applied on an SIW cavity in [15] to implement a wideband planar BPF.

Field perturbation achieved by applying upper surface slots in a triangular-shaped SIW cavity was carried out in [16] to obtain UWB-BPF response. Lastly, a single sector of a 2.2-degree SIW-based cavity was shown in [17] to deliver a dual-mode UWB response.

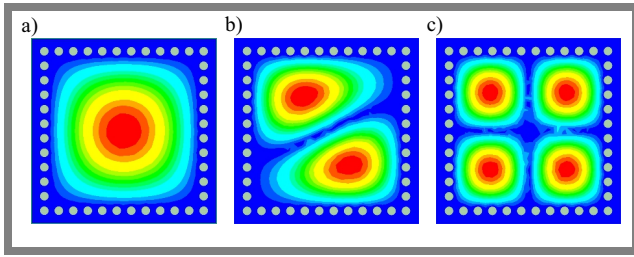


Fig. 1. Distribution of fields in an SIW cavity: a) fundamental mode, b) second mode, and c) fourth mode.

This paper presents a four-pole planar HMSIW filter with UWB-BPF response, where three slots were embedded on the top of the resonator to apply the miniaturization effect to the design. A notch response (NR) was implemented within the passband.

2. Filter Design

Field distribution is a crucial factor in the design of any SIW filter. The distribution of fields is affected by the mode in which the resonator is being excited at. Typically, an SIW cavity is constructed with the use of walls of metallic vias through which the traveling electromagnetic wave is guided and confined within the used substrate. The modes at which the SIW resonator works are transverse electric modes (TE). Ansys EDT simulator software was used to carry out the design and evaluation processes. Figure 1 shows the distribution of the electric field within an SIW cavity model.

Primarily, to design an SIW resonator, the following equations from [18], [19] can be used:

$$p \leq 2d, \tag{1}$$

$$0.05 < \frac{p}{\lambda_c} < 0.25, \tag{2}$$

$$d < \frac{\lambda_g}{5}, \tag{3}$$

$$f_{c(TE_{mn})} = \frac{c}{2\pi} \sqrt{\left(\frac{\pi m}{W}\right)^2 + \left(\frac{\pi n}{L}\right)^2}, \tag{4}$$

$$W = W_{siw} - \frac{d^2}{0.95p}, \tag{5}$$

$$L = L_{siw} - \frac{d^2}{0.95p}. \tag{6}$$

In Eqs. (1)–(6), p is the pitch between two vias (measured from the center of the vias), d is the diameter of each via, λ_g is the guided wavelength, m and n are mode numbers with respect to the TE mode. Parameter W stands for the effective width, W_{SIW} is the width of the SIW, L is the effective length, and L_{SIW} is the length of the SIW.

To miniaturize the SIW structure, a half-mode technique has been used, where the width of the HMSIW cavity becomes $\frac{W}{2}$ [20]. In this filter design, the Rogers RO4003 substrate with relative permittivity $\epsilon_r = 3.55$, loss tangent $\tan \delta = 0.0027$,

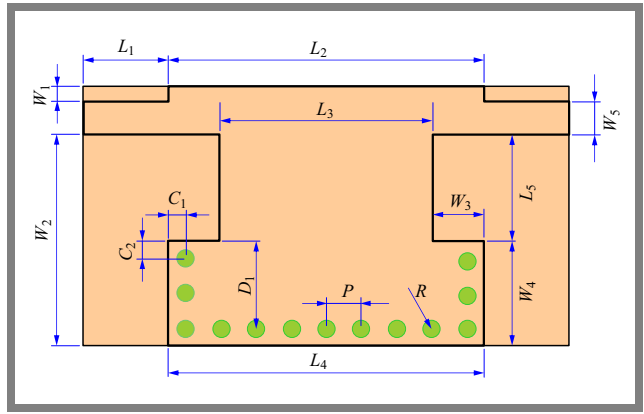


Fig. 2. Initial filter design.

Tab. 1. Dimensions of the initial design (all in mm).

Desc.	Value	Desc.	Value	Desc.	Value
L_1	3.8	W_1	0.5	R	0.3
L_2	10.8	W_2	7.227	P	1.2
L_3	7.3	W_3	1.7	D_1	2.9
L_4	10.8	W_4	3.5	C_1	0.6
L_5	3.465	W_5	1.13	C_2	0.6

and height $h = 0.508$ mm was used. The initial structure is based on Eqs. (1)–(6) and is shown in Fig. 2. The dimensions are listed in Tab. 1.

The response of the initial design is shown in Fig. 3. It can be noticed that the lower cut-off frequency f_1 is 5.1 GHz, while the upper cut-off frequency f_2 is located at 15.5 GHz. Furthermore, the passband response suffers from rippling, which degrades the performance of the filter. In other words, the filter shows a higher insertion loss (IL) in a specific part of the passband region. Additionally, the signal reflection at the ports is too high due to the band performance being driven by the S_{11} response.

To further miniaturize and improve the proposed filter, resonators were loaded onto the top layer of the SIW with complementary T-shaped and U-shaped slots, as illustrated in

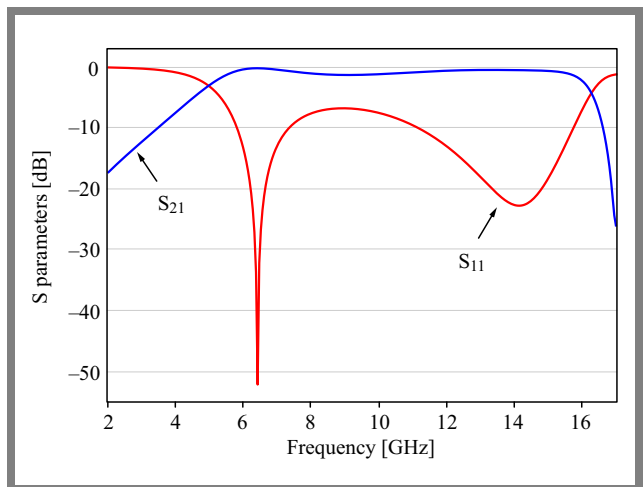


Fig. 3. S_{11} and S_{21} parameters of the initial design.

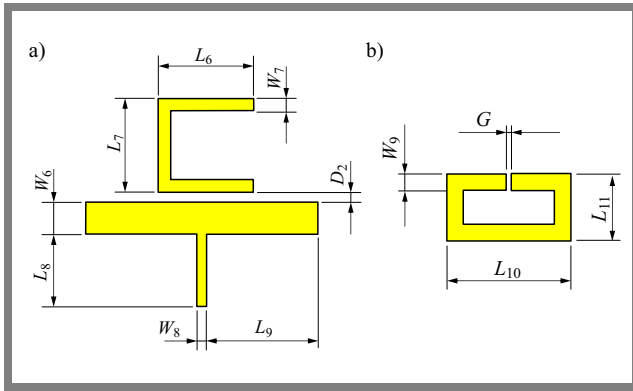


Fig. 4. Modification of the slots and dimensions of the design.

Tab. 2. Dimensions of the coupling slots (all in mm).

Desc.	Value	Desc.	Value	Desc.	Value
W_6	1	L_6	2.95	L_{10}	2.6
W_7	0.4	L_7	2.9	L_{11}	1.4
W_8	0.3	L_8	2.25	D_2	0.3
W_9	0.35	L_9	3.45	G_1	0.1

Fig. 4a. Furthermore, to increase the order of the filter and enhance its response, two HMSIW resonators were used, and a coupling complementary open-ring slot was added between them. The coupling slot with its parameter notations is shown in Fig. 4b, while the parameters of the slots are listed in Tab. 2.

Such a modified UWB-BPF filter structure is depicted in Fig. 5, with its dimensions presented in Tab. 3.

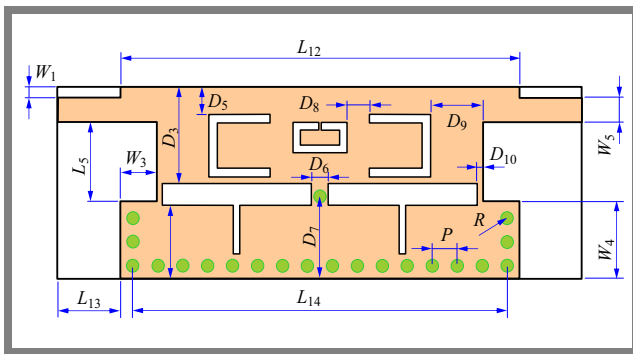


Fig. 5. Improved UWB-BPF.

Tab. 3. Dimensions of the proposed UWB-BPF (all in mm).

Desc.	Value	Desc.	Value	Desc.	Value
L_{12}	19.2	D_4	2.95	D_8	2.6
L_{13}	3.8	D_5	1.26	D_9	2.45
L_{14}	18	D_6	1	D_{10}	0.2
D_3	4.465	D_7	3.8		

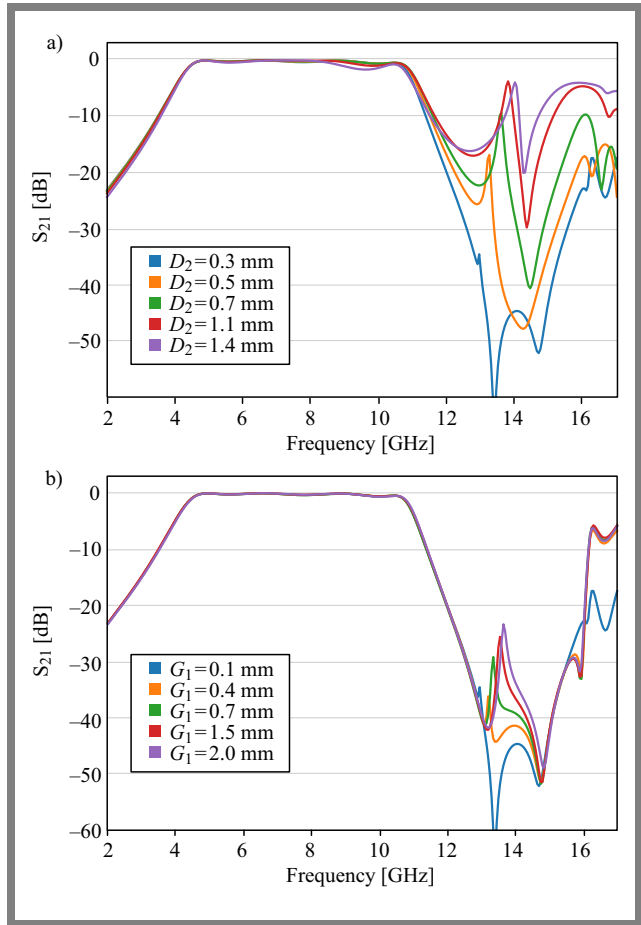


Fig. 6. S_{21} versus frequency for various D_2 and G_1 values.

3. Design Analysis

To achieve the best performance of the proposed filter, a set of parametric studies were performed. This research helps to find the design parameters that have the greatest effect on the filter's response. Mainly, parameters D_2 , G_1 , L_7 , L_9 , D_2 and W_4 are the ones with significant impact on the BPF response. It can be noticed that changes in D_2 and G_1 improve the out-of-band rejection (OBR) response, which is very important to suppress resonance harmonics. However, it is clear that D_2 has the strongest impact on OBR, as illustrated in Fig. 6.

Then parameter L_7 was varied, influencing the location of the upper band cutoff frequency (UBCF). As shown in Fig. 7, an increase in L_7 results in shifting UBCF to lower values, without impact on the lower band cutoff frequency (LBCF). In other words, the bandwidth of this filter can be modified without changing LBCF.

The next analysis proves that changing L_9 affects the location of LBCF, while UBCF remains the same. It can be concluded that an increase in L_9 lowers LBCF, which allows to minimize the filter's size and makes it more suitable for use in space constrained devices that require the filter to work with lower frequencies. Figure 8 confirms that, opposite to the impact of L_7 , an increase in L_9 also leads to a higher bandwidth response.

In conjunction with the reflection coefficient at the designated ports of the proposed filter, it can be determined that parameter W_4 has the biggest impact on S_{11} response, as presented in Fig. 9.

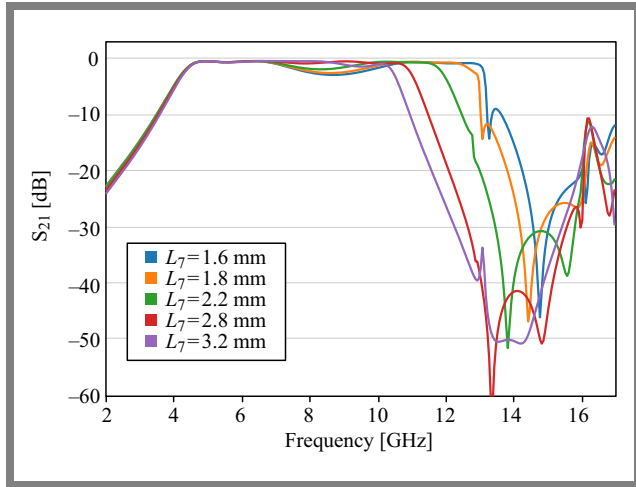


Fig. 7. Impact on S_{21} caused by variation of L_7 parameter.

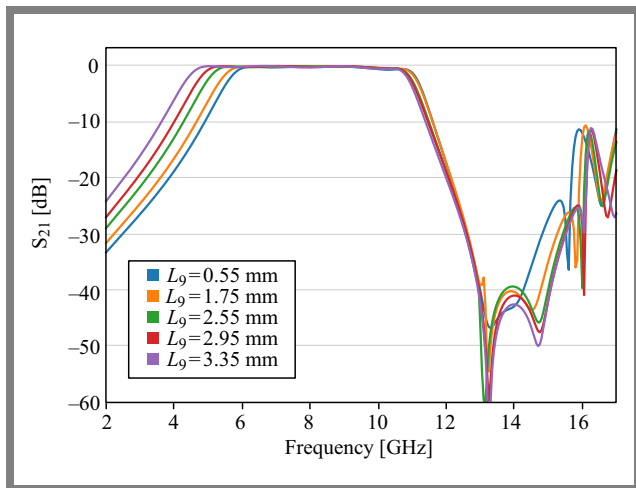


Fig. 8. Study of the L_9 parameter.

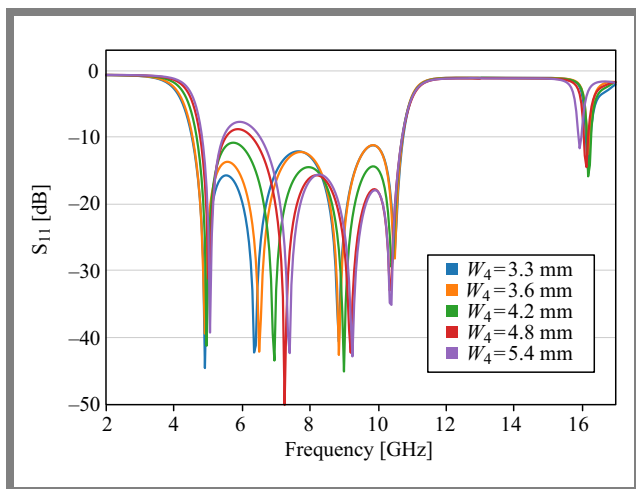


Fig. 9. S_{11} parameter versus frequency with variable W_4 .

4. Design Optimization

To enhance filter response, a search-based multi-objective optimization technique available in the Ansys EDT simulator was utilized. The criteria were set to have the minimum possible insertion loss (IL) with the return loss (RL) greater than 20 dB across the passband.

Such a condition aims to minimize power losses suffered while passing through the filter and to diminish the reflection at the ports of the proposed filter for the entire required passband. $L_1, L_5, W_3, W_4, D_1, D_6, D_8, D_9$ and D_{10} parameters were used in the optimization.

The simulation findings of the proposed BPF are shown in Fig. 10, where $f_1 = 4.12$ GHz and $f_2 = 11$ GHz. IL is found to be better than 0.3 dB with RL over 19 dB. Furthermore, two transmission zeros were realized at 13.66 GHz and 14.68 GHz. This helps to achieve an improved wideband rejection behavior, where it spans for 5.24 GHz after f_2 with rejection of up to 50 dB.

The proposed UWB-BPF has a center frequency (CF) of 7.56 GHz and FBW of 91%. The filter size is calculated to be 18×8.265 mm, or $0.348 \times 0.758 \lambda_g$, where λ_g is the guided wave length at the filter CF.

4.1. In-band Rejection Response

For any UWB-BF, it is important to have an NR in the passband (or band-stop behavior). This is a necessary step to suppress some signals that lie within bands that are required to be blocked due to regulatory compliance.

To produce NR, a modification must be applied to the proposed filter by loading the excitation ends of the filter with L-shaped shunt resonators, where they were integrated within the inset slots to maintain the same proposed filter size. The modified filter design structure is demonstrated in Fig. 11 and its characteristic dimensions are listed in Tab. 4.

A parametric study was conducted to examine the design parameter that has the most impact on NR. Figures 12-13 illustrate the variation in width W_S and length L_S of the L-shaped shunt resonators. One may notice that increasing

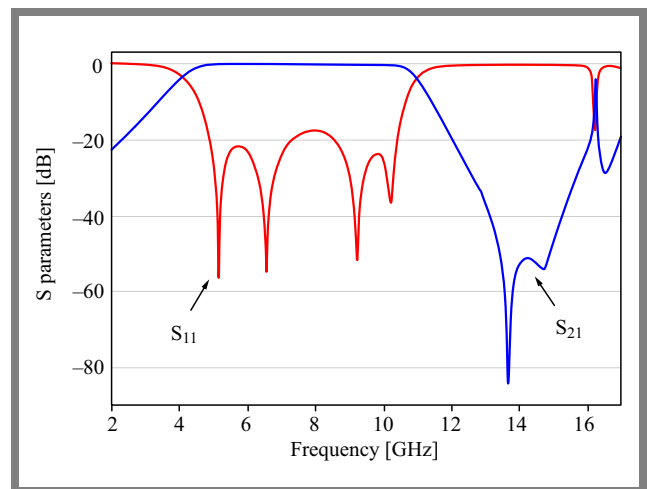


Fig. 10. Response of the S parameters of the proposed UWB-BPF.

W_S and L_S leads to moving NR to lower frequencies, with almost no effect on any other regions in the filter's response. However, W_S variations tend to be more effective in shifting the location of NR to frequencies lower than that of L_S .

Frequency response of the proposed filter is presented in Fig. 14. By comparing the results shown in Figs. 10 and 14, one may conclude that the response of the modified UWB-BPF matches that of the originally proposed UWB-BPF, except at the location where the notch was applied.

In the next step, the Ansys EDT simulator was utilized to plot the electric field (EF) of selected frequencies. EFs at 2 GHz and 13.35 GHz, where no power was transferred through the filter, are illustrated in Figs. 15a and 15d, respectively. For the in-band region, EFs at 6.35 GHz and 10.5 GHz are shown in Figs. 15b-c.

Moreover, Fig. 15e illustrates the EF at which the notch was generated, where the notch is trapped in the notch structure and no power was transferred between the input and output ports.

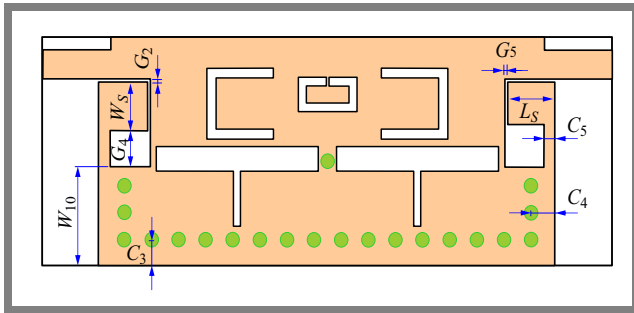


Fig. 11. Modified UWB-BPF structure.

Tab. 4. Characteristic dimensions of the modified UWB-BPF (all in mm).

Desc.	Value	Desc.	Value	Desc.	Value
G_2	0.1	C_3	0.6	W_{10}	3.5
G_3	0.1	C_4	0.8	L_S	1.8
G_4	3.265	C_5	0.2	W_S	0.2

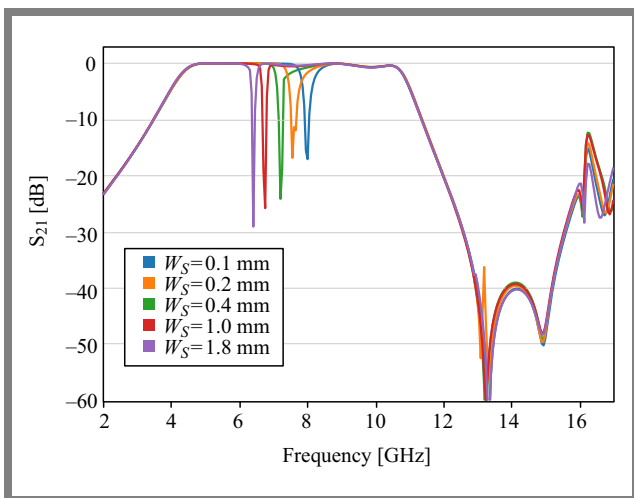


Fig. 12. Parametric study concerning W_S .

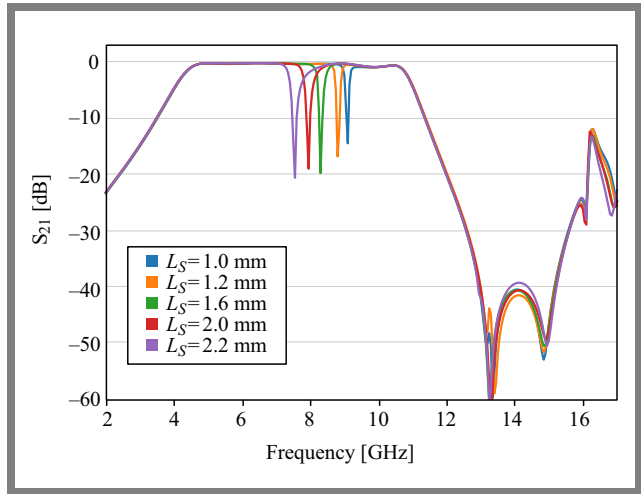


Fig. 13. Parametric study concerning the L_S parameter.

5. Experimental Evaluation and Verification

To validate the Ansys EDT simulated UWB-BPF responses, the proposed filter and its modified version were also simulated in Keysight ADS software (a 2.5D momentum EM simulator). The responses of the filters were in alignment with the findings obtained using Ansys EDT. Figure 16 illustrates the responses of the proposed UWB-BPF obtained using Ansys EDT and Keysight ADS.

It may be concluded that the very small differences between the two findings (Figs. 10, 14 and Figs. 16, 17) come from how the two EM simulators calculated the designs and the methods that were being used to solve the proposed structures. Being a full-wave simulator, Ansys EDT uses the finite element method (FEM), whereas Keysight ADS relies on the method of momentum (MoM) to solve the EM structures, hence the variations shown above.

Table 5 provides a detailed comparison between the most recent published work and the proposed filter. One may summarize that the designed filter structure achieved IL and RL parameters that were better than those obtained by

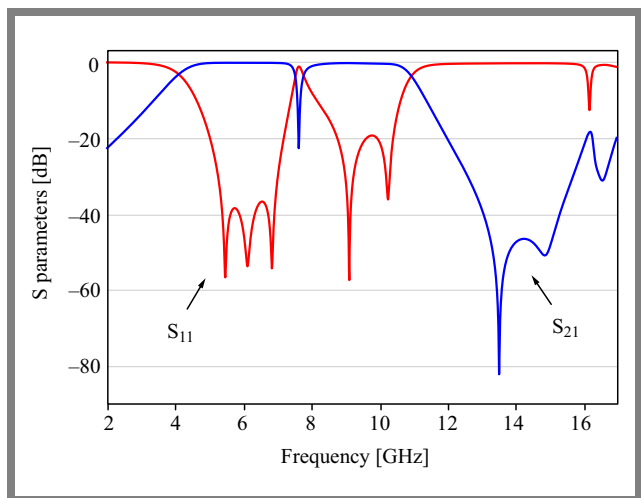


Fig. 14. Response of the S parameters of the modified UWB-BPF.

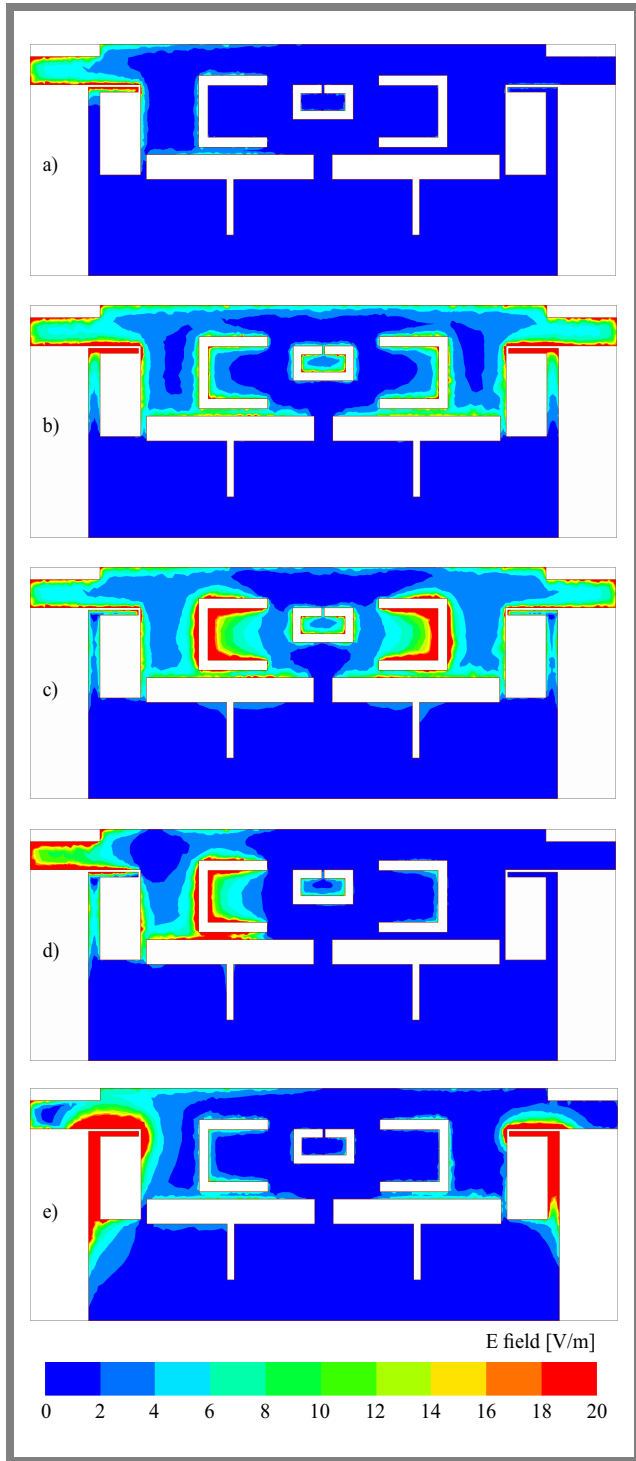


Fig. 15. Electric field at: a) 2 GHz, b) 6.35 GHz, c) 10.50 GHz d) 13.35 GHz, and e) 7.6 GHz.

most of its counterparts. Furthermore, the proposed filter is characterized by a smaller size in comparison with [3], [4], [6], but is larger when compared with [21].

6. Conclusions

In this paper, a UWB-BPF based on HMSIW and loaded with three different-shaped slots was proposed. The filter operates

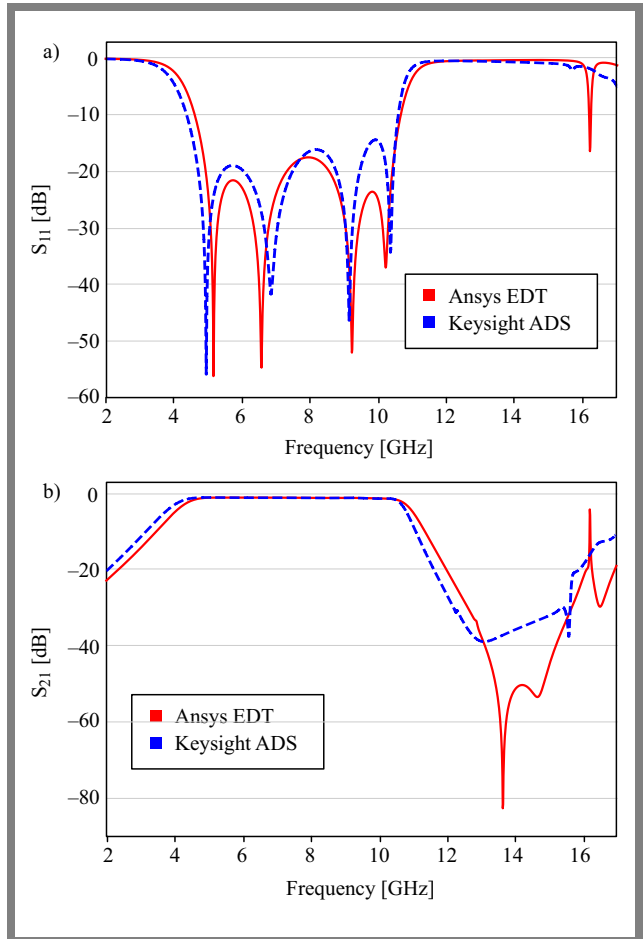


Fig. 16. S parameters of the proposed UWB-BPF obtained with Ansys EDT and Keysight ADS simulators: a) S_{11} and b) S_{21} .

in the frequency band between 4.12 GHz and a 11 GHz, with FBW of 91% and a low IL level of 0.3 dB at the CF. Its RL is better than 19 dB. The structure was designed with a small filter area of $0.26 \lambda_g^2$ making it suitable for modern compact systems.

Moreover, integrated L-shaped slots were included within the same filter area to introduce an NR through the passband region. Compared with filters described in works published earlier, the proposed solution achieved a stronger overall balance of bandwidth, loss, and size.

Tab. 5. Comparison with other works.

Ref.	CF [GHz]	FBW [%]	IL [%]	RL [%]	Size [λ_g]
[3]	6.6	106	< 1.8	> 10	0.37
[4]	6.7	107	< 1.6	> 15	0.37
[6]	11.65	119	< 0.3	> 20	0.29
[21]	6.5	92	< 1.74	> 15	0.24
This paper	7.56	91	< 0.3	> 19	0.26

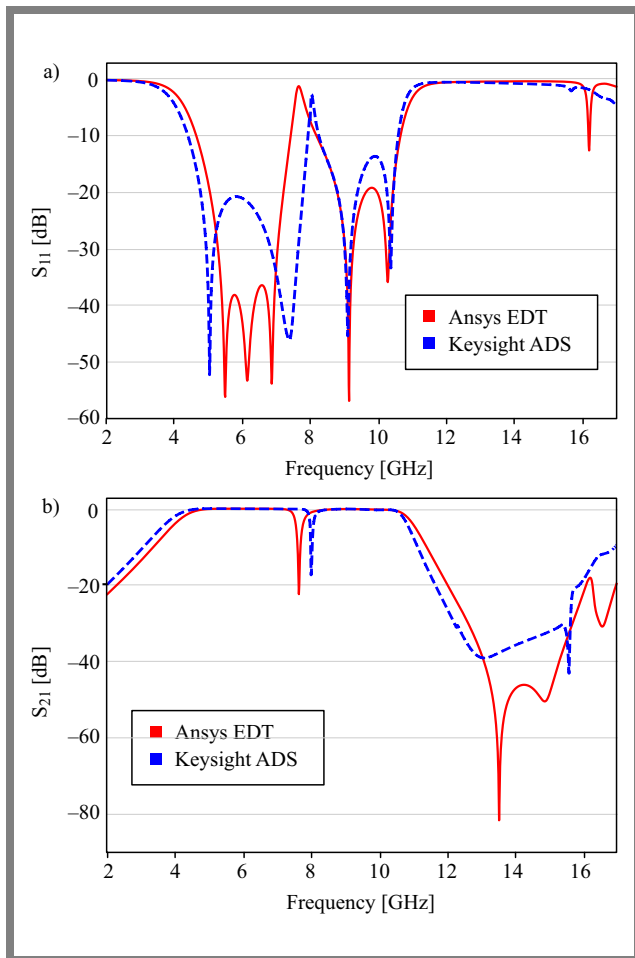


Fig. 17. S parameters of the modified UWB-BPF obtained with Ansys EDT and Keysight ADS simulators: a) S_{11} and b) S_{21} .

References

- [1] Code of Federal Regulations, *Part 15: Radio Frequency Devices*, 2023 [Online]. Available: <https://www.ecfr.gov/current/title-47/part-15>.
- [2] R.P. Verma and B. Sahu, "Structure and Performance Comparison of Ultra-wideband Bandpass Filter: Review Article", *2021 7th International Conference on Signal Processing and Communication (ICSC)*, Noida, India, 2021 (<https://doi.org/10.1109/ICSC53193.2021.9673323>).
- [3] S. Udhayanan and K. Shambavi, "Compact Single Notch UWB Bandpass Filter with Metamaterial and SIW Technique", *PIER Letters*, vol. 117, pp. 41–46, 2024 (<https://doi.org/10.2528/PIERL23113004>).
- [4] S. Udhayanan and K. Shambavi, "Metamaterial-based Compact UWB Bandpass Filter Using Substrate Integrated Waveguide", *PIER Letters*, vol. 120, pp. 1–6, 2024 (<https://doi.org/10.2528/PIERL24031107>).
- [5] Z. Li *et al.*, "A Miniaturized Ultra-wideband Dual Bandpass Frequency Selective Surface with High Selectivity", *IEEE Transactions on Antennas and Propagation*, vol. 72, pp. 6510–6519, 2024 (<https://doi.org/10.1109/TAP.2024.3423322>).
- [6] C. Li *et al.*, "An Ultra-wideband Bandpass Filter Based on Half-mode Substrate Integrated Waveguide Loaded with Rectangular-ring Slot", *2022 10th International Symposium on Next-Generation Electronics (ISNE)*, Wuxi, China, 2023 (<https://doi.org/10.1109/ISNE56211.2023.10221607>).
- [7] S. Keelailam *et al.*, "A Wideband Bandpass Filter Using U-shaped Slots on SIW with two Notches at 8 GHz and 10 GHz", *2022 IEEE*

International Conference on Signal Processing and Communications (SPCOM), Bangalore, India, 2022 (<https://doi.org/10.1109/SPCOM55316.2022.9840774>).

- [8] Y.-F. Xie, Y.-H. Ma, and W.-S. Zhao, "A Single-notch Ultra-wideband Bandpass Filter Based on Bow-tie Cells", *2023 IEEE International Workshop on Electromagnetics: Applications and Student Innovation Competition (iWEM)*, Harbin, China, 2023 (<https://doi.org/10.1109/iWEM58222.2023.10234900>).
- [9] V.P.K. Kanaparthi, V.K. Velidi, R. Rajkumar, and R.R.T., "A Compact Ultra-wideband Multimode Bandpass Filter with Sharp-rejection Using Stepped Impedance Open Stub and Series Transformers", *IEEE Transactions on Circuits and Systems II*, vol. 69, pp. 4824–4828, 2022 (<https://doi.org/10.1109/TCSII.2022.3192512>).
- [10] T. Duraisamy *et al.*, "Compact Wideband SIW Based Bandpass Filter for X, Ku and K Band Applications", *Radioengineering*, vol. 30, pp. 288–295, 2021 (<https://doi.org/10.13164/re.2021.0288>).
- [11] K. Mahant *et al.*, "Spoof Surface Plasmon Polaritons and Half-mode Substrate Integrated Waveguide Based Compact Band-pass Filter for Radar Application", *PIER M*, vol. 101, pp. 25–35, 2021 (<https://doi.org/10.2528/PIERM20121803>).
- [12] R.S. Sangam and R.S. Kshetrimayum, "Hybrid Spoof Surface Plasmon Polariton and Substrate Integrated Waveguide Bandpass Filter with High Out-of-band Rejection for X-band Applications", *IET Microwaves Antennas and Propagation*, vol. 15, pp. 289–299, 2021 (<https://doi.org/10.1049/mia2.12049>).
- [13] E.M. Messaoudi, J.D. Martinez, and V.E. Boria, "Miniaturized Ultra-wideband Bandpass Filter Based on Substrate Integrated Quasi-lumped Resonators", *2021 IEEE MTT-S International Microwave Filter Workshop (IMFW)*, Perugia, Italy, 2021 (<https://doi.org/10.1109/IMFW49589.2021.9642382>).
- [14] N. Muchhal *et al.*, "Design of Hybrid Fractal Integrated Half Mode SIW Band Pass Filter with CSRR and Minkowski Defected Ground Structure for Sub-6 GHz 5G Applications", *Photonics*, vol. 9, art. no. 898, 2022 (<https://doi.org/10.3390/photonics9120898>).
- [15] A.J. Salim *et al.*, "Miniaturized SIW Wideband BPF Based on Folded Ring and Meander Line Slot for Wireless Applications", *2017 Second Al-Sadiq International Conference on Multidisciplinary in IT and Communication Science and Applications (AIC-MITCSA)*, Baghdad, Iraq, 2017 (<https://doi.org/10.1109/AIC-MITCSA.2017.8722992>).
- [16] W. Fu *et al.*, "Compact Bandpass Filter Based on Single Isosceles Right Triangular Substrate Integrated Waveguide Cavity and Modified Complementary Compact Microstrip Resonant Cell", *IEICE Electronics Express*, vol. 18, art. no. 20200397, 2021 (<https://doi.org/10.1587/elex.17.20200397>).
- [17] J. Liu, Y. Zhang, X. Wan, and H. Jing, "Miniaturized Dual-mode Ultra-wideband Filter Using Sector Substrate Integrated Waveguide", *Microwave and Optical Technology Letters*, vol. 63, pp. 2343–2347, 2021 (<https://doi.org/10.1002/mop.32912>).
- [18] D. Deslandes and K. Wu, "Accurate Modeling, Wave Mechanisms, and Design Considerations of a Substrate Integrated Waveguide", *IEEE Transactions on Microwave Theory and Techniques*, vol. 54, pp. 2516–2526, 2006 (<https://doi.org/10.1109/TMTT.2006.875807>).
- [19] Y. Cassivi *et al.*, "Dispersion Characteristics of Substrate Integrated Rectangular Waveguide", *IEEE Microwave and Wireless Components Letters*, vol. 12, pp. 333–335, 2002 (<https://doi.org/10.1109/LMWC.2002.803188>).
- [20] W. Hong *et al.*, "Half Mode Substrate Integrated Waveguide: A New Guided Wave Structure for Microwave and Millimeter Wave Application", *2006 Joint 31st International Conference on Infrared Millimeter Waves and 14th International Conference on Terahertz Electronics*, Shanghai, China, 2006 (<https://doi.org/10.1109/ICIMW.2006.368427>).
- [21] L. Huang and S. Zhang, "Ultra-wideband Ridged Half-mode Folded Substrate-integrated Waveguide Filters", *IEEE Microwave and Wireless Components Letters*, vol. 28, pp. 579–581, 2018 (<https://doi.org/10.1109/LMWC.2018.2835666>).

Hussein Al-Jeshami, M.Sc.

Electromechanical Engineering Department

 <https://orcid.org/0000-0001-7063-754X>

E-mail: hussein.m.abdul@uotechnology.edu.iq

University of Technology – Iraq, Baghdad, Iraq

<https://uotechnology.edu.iq>

Hussam Al-Saedi, Ph.D.

Communication Engineering Department

 <https://orcid.org/0000-0002-2029-7361>

E-mail: hussam.h.ali@uotechnology.edu.iq

University of Technology – Iraq, Baghdad, Iraq

<https://uotechnology.edu.iq>

Mohammed F. Hasan, Ph.D.

Communication Engineering Department

 <https://orcid.org/0000-0002-0244-9595>

E-mail: mohammed.f.hasan@uotechnology.edu.iq

University of Technology – Iraq, Baghdad, Iraq

<https://uotechnology.edu.iq>

Halah I. Khani, M.Sc.

Communication Engineering Department

 <https://orcid.org/0000-0001-5572-1073>

E-mail: halah.i.khani@uotechnology.edu.iq

University of Technology – Iraq, Baghdad, Iraq

<https://uotechnology.edu.iq>

Muhannad Y. Muhsin, Ph.D.

Electrical Engineering Department

 <https://orcid.org/0000-0003-3937-4467>

E-mail: muhannad.y.muhsin@uotechnology.edu.iq

University of Technology – Iraq, Baghdad, Iraq

<https://uotechnology.edu.iq>

Wael M. Abdel-Wahab, Ph.D.

Electrical and Computer Engineering

 <https://orcid.org/0000-0002-0994-3529>

E-mail: wmabdelw@uwaterloo.ca

University of Waterloo, Waterloo, Canada

<https://uwaterloo.ca>